scientific reports

Check for updates

OPEN

Influence of deformation path on microstructure evolution during multi-step deformation of a high strength steel: experiments and FE analysis

Prashant Dhondapure[1]✉, Soumyaranjan Nayak[2], Simin Dourandish[3] & Mohammad Jahazi[1]

This study aims to investigate the effect of deformation path on deformation and microstructure evolution during the multi-step deformation of a high strength steel. The deformation paths were illustrated by flat and concave surface anvils. Multi-step deformation experiments were conducted on high strength steel specimens using thermomechanical simulator, Gleeble 3800 equipped with MaxStrain module, a special purpose attachment. All tests were performed at a strain rate and temperature of 0.01 s^{-1} and 1150 °C respectively, considering two deformation paths. A total true strain of 0.84 was imparted over four steps, with approximately 0.21 strain applied per step. The results were used to analyze the influence of varying deformation paths on microstructure evolution and hardness distribution. A finite element (FE) model was developed using Forge NxT 3.2 FE code to simulate the multi-step deformation process. The strain distribution obtained via FE model was correlated to the average grain size and hardness distribution after the multi-step deformation experiments for validation. This validated FE model was capable of predicting strain distribution, dynamic recrystallization (DRX) volume fraction, and grain size evolution during the multi-step deformation process. A comparative study of results obtained from two deformation paths was conducted to determine the optimal deformation path, aiming homogeneous strain and grain size distribution. The Coefficient of Variation (CoV) was used to assess the heterogeneity of the hardness distribution. The results suggest that concave anvils promote a higher and more uniform strain distribution, leading to a homogeneous distribution of grain size and hardness. An increased and more uniform strain distribution promotes complete dynamic recrystallization (DRX) with finer grain size leading to homogeneous hardness distribution.

Keywords Gleeble 3800 maxstrain, Multi-step deformation, Deformation paths, FE analysis, Microstructure evolution, Mechanical properties

In recent years, demand for large size components has increased in automobile and transport industry. This has resulted in an increased demand for large size dies and plastic injection molds that would allow fabrication of very large size bumpers and dash boards. High strength forged steels are used for the fabrication of large size molds and dies for extrusion or plastic injection technologies. The manufacturing of preform for mold and die involves casting, open die forging, heat treatment and machining to obtain desired shapes[1–4]. During the casting and forging, *single* and *multi-step*, process inhomogeneities arise due to temperature gradient and non-uniform deformation leading to variations in microstructure and mechanical properties distribution throughout the thickness of the final products[5–8]. Large forged ingots are often characterized by undesirably large grains at their center. One objective of present work is to develop a method for reducing grain size in the core of the forged blocks. Nevertheless, for larger ingots, particularly those exceeding 800 mm in diameter and thickness, grain size distribution is often non-uniform. This inhomogeneity can result in inconsistent mechanical properties,

[1]Department of Mechanical Engineering, École de Technologie Supérieure, 1100 Notre Dame West, Montreal, QC H3C 1K3, Canada. [2]Advanced Forming Research Centre (AFRC), University of Strathclyde, 85 Inchinnan Drive, Inchinnan, Renfrewshire PA4 9LJ, UK. [3]Finkl Steel-Sorel Inc., 100 McCarthy, Saint-Joseph-de-Sorel, QC J3R 3M8, Canada. ✉email: dhondapure11@gmail.com

Elements	C	Mo	Mn	Ni	Si	Cr	Balance
Weight%	0.31	0.51	0.90	0.70	0.35	1.85	Fe

Table 1. Chemical configuration of medium carbon low alloy high strength steel[14].

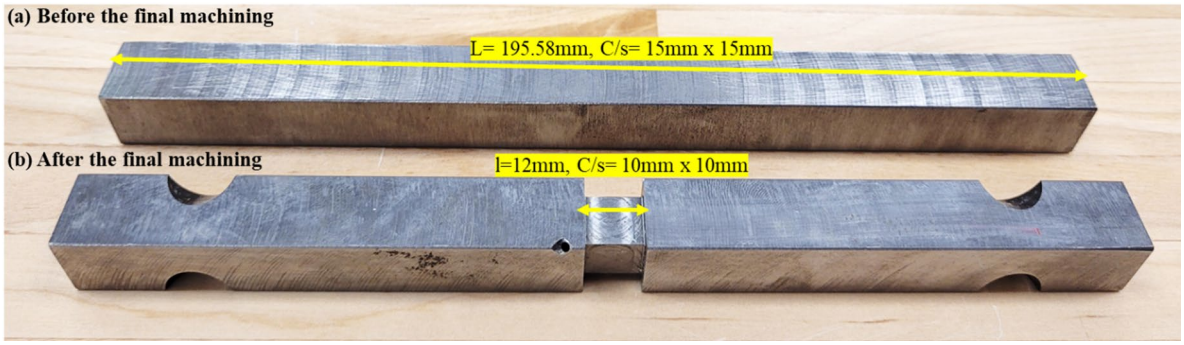

Fig. 1. As received specimen before (**a**) and after (**b**) the final machining of the square cross-section bar received from Finkl Steel.

potentially leading to part rejection[9]. These imperfections become more prominent during manufacturing of large size molds and dies which could lead to part rejection during the quality check[10–13]. The present authors have investigated the effect of different deformation paths on microstructure evolution during *single step* upsetting process of a high strength steel[14]. In the current work, multi-step deformation process is considered, as it allows producing more complex geometries and is pivotal in reducing casting defects[11,12]. Precise control of key thermomechanical parameters, including heating rate, holding time, deformation severity, deformation rate, and machine characteristics, is essential during multi-step deformation to ensure a favorable microstructure and optimal mechanical properties through the thickness of large forgings[15].

In addition to above discussed parameters, the deformation path plays a critical role during the hot metalworking of metals. It has a substantial effect on material flow (i.e., strain distribution) and consequently on metallurgical phenomena like dynamic recovery (DRV) and dynamic recrystallization (DRX), that influence the final grain size of the forged material[6,16–18]. Therefore, designing optimal multi-step forging processes necessitates a deep understanding of how process and geometric parameters interact and affect microstructural development, which ultimately governs final mechanical properties[16,19–22].

The effect of thermomechanical parameters such as deformation temperature, strain rate has been extensively studied, resulting in vast literature detailing the behavior of various materials under the different deformation conditions[20–26]. However, other factors which equally affect the material response to deformation are machine characteristics and die geometry[7,16,27]. In this study, die geometry is considered to provide different deformation paths.

Despite extensive research on the influence of thermomechanical parameters on single step deformation using flat dies, the available studies in the literature on the effect of deformation path on microstructure evolution during multi-step deformation are limited. In particular, publications in open literature on microstructure based FE simulation of multi-step deformation process considering different deformation paths are very limited[27–29]. The present work addresses the above gap in the literature. A combination of physical simulation of multi-step deformation process and numerical simulation was employed in the present study to achieve the goal. Further, a comparative analysis of the impact of dies geometry on microstructure homogeneity of a multi-step deformed specimen has been tried to propose an optimal die geometry for the industrial scale forgings.

Materials and methods

Medium carbon low alloy high strength steel provided by Finkl Steel (Sorel, Quebec, Canada) was used for the present investigation. The elemental composition of the alloy is provided in Table 1.

Specimens for the MaxStrain tests were prepared from a rectangular forged slab of high strength steel of dimension 635 mm x 1986 mm x 2997 mm. As shown in Fig. 1(a) square cross-sectioned bars measuring 15 mm × 15 mm × 195.58 mm were machined from the core of the slab and received from Finkl Steel to perform final machining at ETS, Montreal to achieve the final dimensions shown in Fig. 1(b). These square bars were then further machined to prepare the final MaxStrain specimens. As shown in the Fig. 1(b), square bar machined at middle to convert a 15 mm x 15 mm x 12 mm cross-section into a 10 mm × 10 mm × 12 mm reduced size square cross-section. It must be mentioned that the multi-step deformation in MaxStrain module is applied to the reduced section of the final specimen, as shown in Fig. 1(b).

Multi-step deformation experiments

In this study, flat, and concave surface curvature anvils, shown in Fig. 2, were used for the multi-step deformation experiments. Figure 2a and b show schematic of the anvil geometries with dimensions and final machined anvils from the tungsten carbide rectangular blocks of size 10 mm x 20 mm x 25 mm respectively. Two pair of each anvil set was prepared for testing, to simulate the condition of Flat-Flat and Concave-Concave anvils combination during multi-step deformation process. The surface curvature of concave anvils was optimized with the help of FE analysis to ascertain higher and uniform deformation.

The multi-step deformation experiments employing different deformation paths were performed on Gleeble 3800 with MaxStrain system, experimental setup present in the laboratory at École de Technologie Supérieure (ETS), Montreal, Canada as shown in Fig. 3. This system is developed by Dynamic Systems Inc. (DSI), United States, https://gleeble.com/products/mobile-conversion-units/maxstrain.html. In the Gleeble system, test parameters such as temperature, strain rate and strain can be controlled with high precision during the deformation process. Figure 3b and c provides the view inside the Maxstrain chamber with concave anvils setup and specimen installed inside during the heating to the test temperature respectively.

The multi-step deformation test parameters, including temperature, applied deformation, and strain rate for each step, were selected to reflect actual industrial forging conditions. During the heating and holding steps, prior to deformation, the anvils were positioned approximately 0.5 mm from the specimen to preheat them close to the test temperature, thus minimizing the temperature drop during the multi-step deformation. Numerous trials were performed before conducting the actual tests to establish a reliable thermocouple installation procedure. Super glue and high-temperature white cement were used to secure the thermocouples within the 3 mm diameter holes. This optimized installation method ensured temperature stability with a temperature gradient of less than 5 °C. Figure 4a illustrates the heating, holding, and multi-step deformation cycle used in the experiments. Specimens were heated to 1260 °C, at a rate of 2 °C/s under vacuum to avoid oxidation. A holding time of 5 min was applied to ensure uniform temperature distribution in the specimen. Then, the specimens were cooled to the test temperature of 1150 °C at 1 °C/s, followed by different hits at a strain rate of 0.01 s^{-1}. After the first step of deformation, the specimen was rotated clockwise by 90° around its longitudinal axis and compressed again in a direction perpendicular to the original compression axis. Again, after the second step deformation, it was rotated counterclockwise by 90° to its previous orientation and deformed once more. This cycle was repeated to complete four steps to achieve the required level of deformation, a total true strain of 0.84 in four steps, which amounts to around 0.21 strain per step. At the end of the 4th step, the specimens underwent chamber cooling under the vacuum. Figure 4b shows the MaxStrain specimen before and after the multi-step deformation process. At the cross-sectional dimensions of the specimens deformed using the flat and concave anvils were 8.98 × 9.10 mm and 9.44 × 9.21 mm, respectively. Furthermore, the multi-step deformed specimens

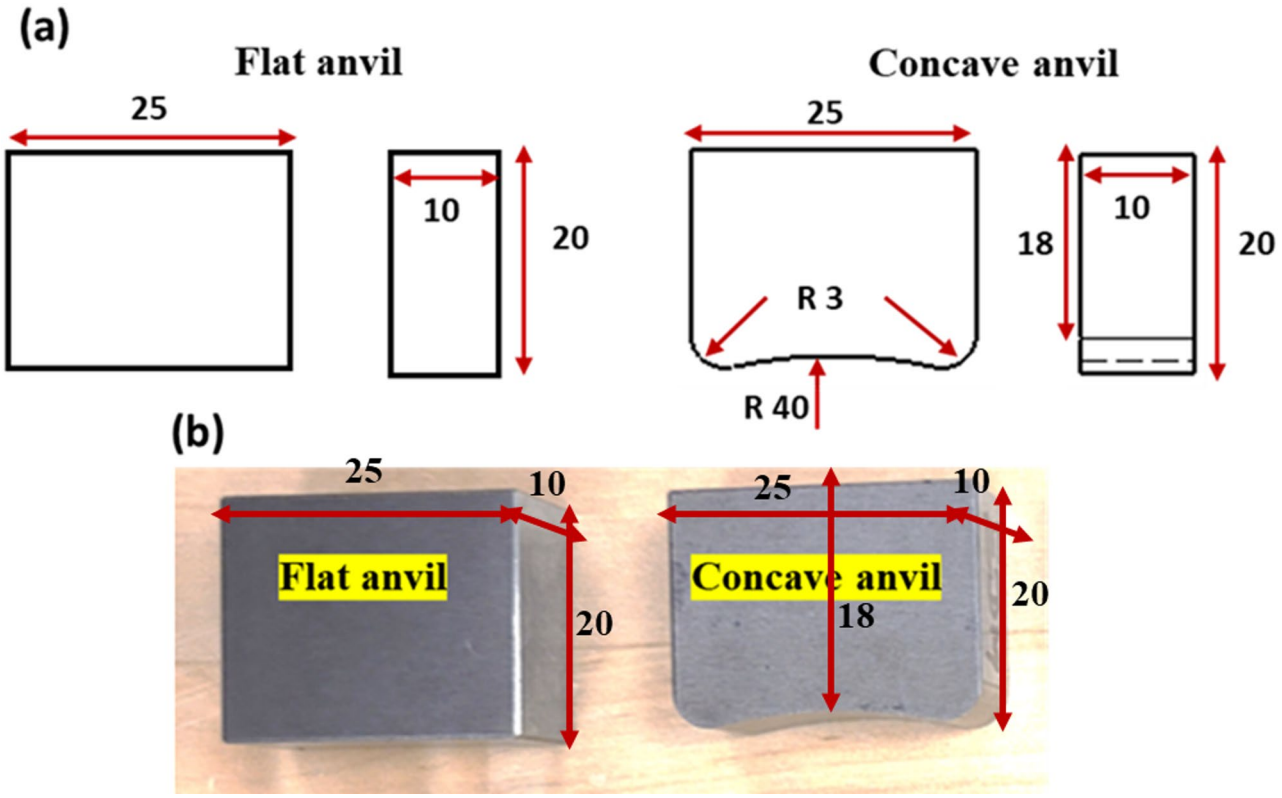

Fig. 2. **(a)** Schematic of anvil geometries with their dimensions and, **(b)** Final machined anvils of tungsten carbide (all dimensions are in mm).

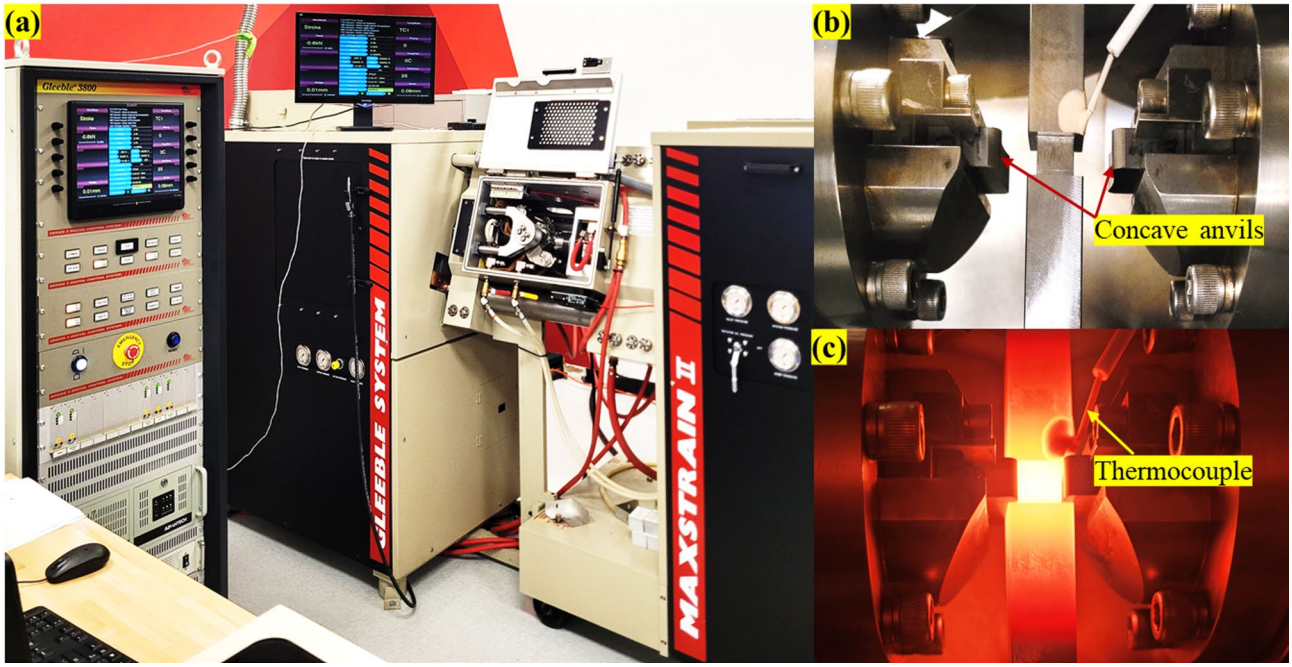

Fig. 3. Experimental setup for multi-step deformation: (**a**) Gleeble 3800 with MaxStrain module, (**b**) Experimental setup with concave anvils, specimen with installed thermocouple and, (**c**) View inside the vacuum chamber during testing.

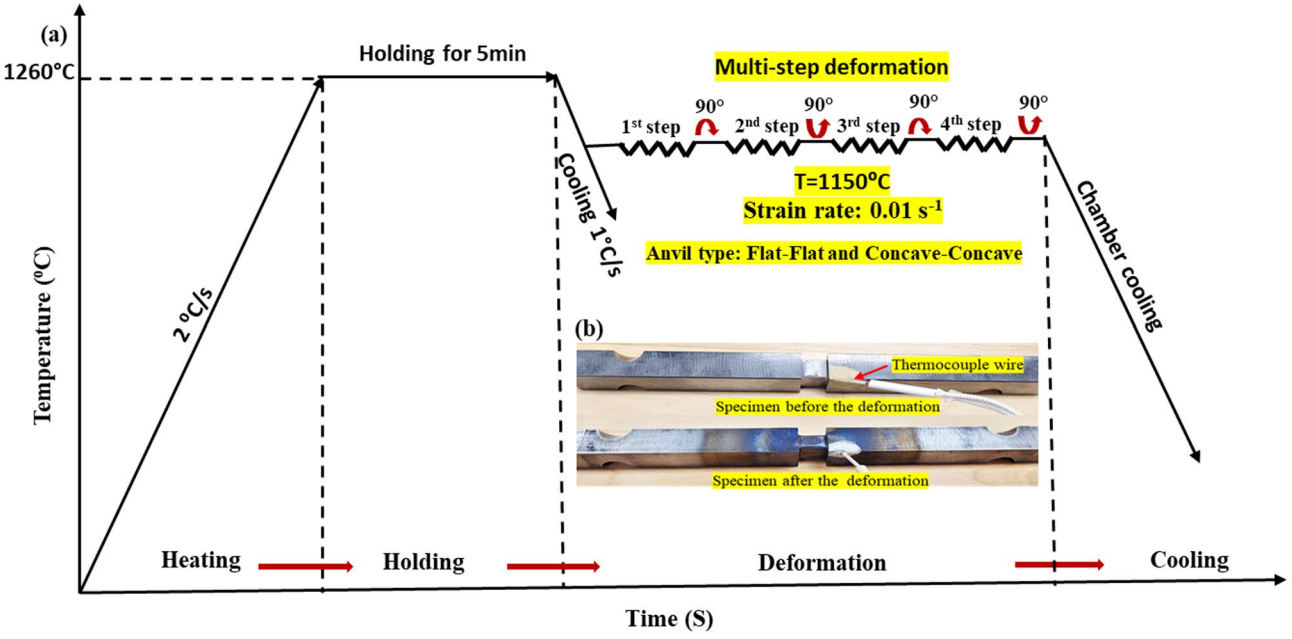

Fig. 4. (**a**) Schematic of multi-step deformation testing cycle using MaxStrain module and, (**b**) Represents specimen before and after the deformation.

were characterized and compared to evaluate the effect of different deformation paths on grain size and hardness value variation.

Following the multi-step deformation testing, specimens were sectioned parallel to the deformation axis for microstructure analysis and grain size measurement. The cut specimens were then hot mounted for polishing. Standard polishing techniques were employed for surface preparation prior to chemical etching. To reveal the grain boundaries in the multi-step deformed specimens, an etchant consisting of saturated picric acid and sodium dodecyl benzene sulfonate was used: 100 ml of saturated picric acid, 0.5 g of sodium dodecyl benzene

sulfonate, and 3–4 drops of HCl[30,31]. The etchant was applied at room temperature for 3 to 5 min to reveal the prior austenite grain boundaries. Using the laser confocal microscope, optical micrographs were taken for microstructure comparison and grain size measurement. The average grain size was determined according to standard ASTM E112[32]. In addition, detailed explanation of the metallographic procedures and techniques used can be found in recent research published by the authors[14].

Material and microstructure model

In order to ascertain the material model which could accurately predict flow stress across different temperatures and strain rates, several constitutive models (Arrhenius, Hensel–Spittel, and Johnson–Cook) were evaluated, and their predictive accuracy compared in our previous work[14]. The results of this comparison indicated that the Arrhenius model offered superior predictions for the investigated steel compared to the Hansel-Spittel and Johnson-Cook models. A modified strain compensated Arrhenius model was used, in which the material constants A, α, n and Q, were expressed as fourth order polynomial functions of strain[14]. The resulting constitutive relation linking flow stress to strain rate, temperature, and strain-dependent activation energy is outlined below[3,33].

$$\sigma\ (y) = \frac{1}{\alpha\ (\epsilon\ )} ln \left\{ \left(\frac{Z\ (\epsilon\ )}{A\ (\epsilon\ )} \right)^{\frac{1}{n(\epsilon\ )}} + \sqrt{\left(\frac{Z\ (\epsilon\ )}{A\ (\epsilon\ )} \right)^{\frac{2}{n(\epsilon\ )}} + 1} \right\} \tag{1}$$

$$Z = \dot{\epsilon}\, exp\left(\frac{Q}{RT}\right) = A[sinh\ (\alpha\ \sigma\ )]^n \tag{2}$$

In Eqs. 1 and 2, Z represents the Zener-Hollomon parameter, and Q signifies the activation energy necessary to overcome resistance to deformation. The material specific constants are denoted by A, α, and n, while R represents the universal gas constant. Temperature is represented by T, strain rate by $\dot{\epsilon}$, and applied stress by σ.

It is widely accepted that during the hot metal working process microstructure evolution is mainly governed by three phenomena: work hardening, dynamic recovery (DRV) and dynamic recrystallization (DRX). In materials with low stacking fault energy (SFE), DRX is the primary softening mechanism, typically occurring after a critical deformation threshold was reached[30]. The DRX volume fraction is a function of strain, strain rate, deformation temperature, and initial grain size and can be modeled using the Johnson-Mehl-Avrami-Kolmogoro (JMAK) equation, where the Avrami coefficient (b) and Avrami exponent (n) describes the nucleation and growth kinetics of recrystallized grains[14,31]:

$$X = 1 - e^{-b.t^n} \tag{3}$$

Here, b and n represent the Avrami coefficients. We have implemented the JMAK model in the present research to predict microstructure. Both the developed material and microstructure models were integrated into the Forge NxT 3.2 finite element software to effectively replicate microstructure evolution of the large size block during multi-step forging. Further details regarding the determination of model constants and the model integration process can be found in our recent publication[14,34]. Table 2 presents the expressions and parameters used to predict the DRX volume fraction, DRX grain size and grain growth during hot deformation of high strength steel. In the below expression, t represents the time from the start of grain growth, T (°C) gives the deformation temperature, d_0 (μm) initial grain size and d_{gg} (μm) is the final grain size (grown average grain size).

FE modeling of multi-step deformation process

The multi-step deformation process was simulated using Finite Element (FE) code Forge NxT 3.2. A 3D FE model was used for this analysis. Figure 5 shows the FE model with mesh geometry used for the simulation of the multi-step deformation process. Two different anvil surface curvatures were used in the present investigations, as shown Fig. 2. FE model with two anvil geometries, flat and concave were used for simulation as shown in Fig. 5a and b respectively. Tetrahedron four node mesh type was used for the meshing and mesh sensitivity analysis was done to optimize the mesh size. Table 3 provides detail input boundary conditions and specimen dimensions used for this analysis. Boundary conditions used for the FE analysis were determined based on the industrial data and previous study done by the present authors[14]. This includes the total amount of deformation, temperature, strain rate, heat transfer coefficient, friction coefficient, material and microstructure model. In this

Parameters	Equations
Dynamic recrystallization fraction	$X_{drx} = 1 - \exp\left(-0.318\left(\frac{\epsilon - \epsilon_c}{\epsilon_{0.5}}\right)^3\right)$
Recrystallized Grain size	$D_{drx} = 14\,\dot{\epsilon}^{0.07} Z^{-0.205} \exp\left(\frac{-42327}{R.T}\right).X_{drx}^{0.21}$
Grain Growth	$d_{gg}^{4.7} - d_0^{4.7} = 1.41 \times 10^{23} \exp\left(\frac{-43927}{R.T}\right).t$

Table 2. Provides expression used for DRX prediction for high strength steel[14,34,35].

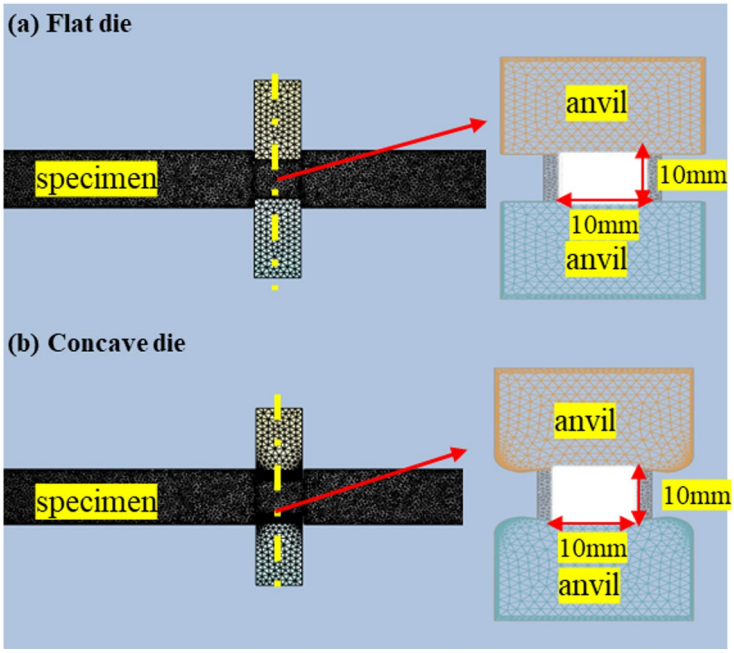

Fig. 5. Shows the FE model with: (**a**) Flat anvils and, (**b**) Concave anvils.

Parameters	Input boundary conditions
Size of deformation region (mm)	10 × 10 × 12
Type of anvils (upper and lower)	Flat-Flat and Concave-Concave
Specimen initial temperature (^{0}C)	1150
Die temperature (^{0}C)	≈1150
Deformation rate (s^{-1})	0.01
Ingot material	Modified AISI P20 steel
Material model	Arrhenius
Microstructure model	JAMK
Total number of steps	4
Deformation per step	≈0.21
Total deformation	≈0.84
Mesh size (mm)	0.7 (tetrahedron)
Friction coefficient	0.8

Table 3. Input boundary conditions used for numerical simulation of multi-step deformation.

FE model, dry contact was assumed between the tungsten carbide anvils and the workpiece i.e., no lubricant was used. Accordingly, selected a friction coefficient of 0.8, based on industry standards for clean, dry tungsten carbide steel interfaces[36]. The heat transfer coefficient (HTC) for the thermal modelling at the die-workpiece interface was based on the medium interaction settings provided by Forge NxT's material library. HTC under forging pressure was chosen to be 10,000 W/(m²·K) to simulate hot forming applications[7,35].

Results and discussion

Equivalent plastic strain distribution

Figure 6 shows the FE analysis results for equivalent plastic strain distribution at end of multi-step deformation process with flat and concave anvils. This study found that modifying the die surface curvature significantly affected strain distributed in the core of the hot deformed specimens. Flat anvils resulted in strain values ranging

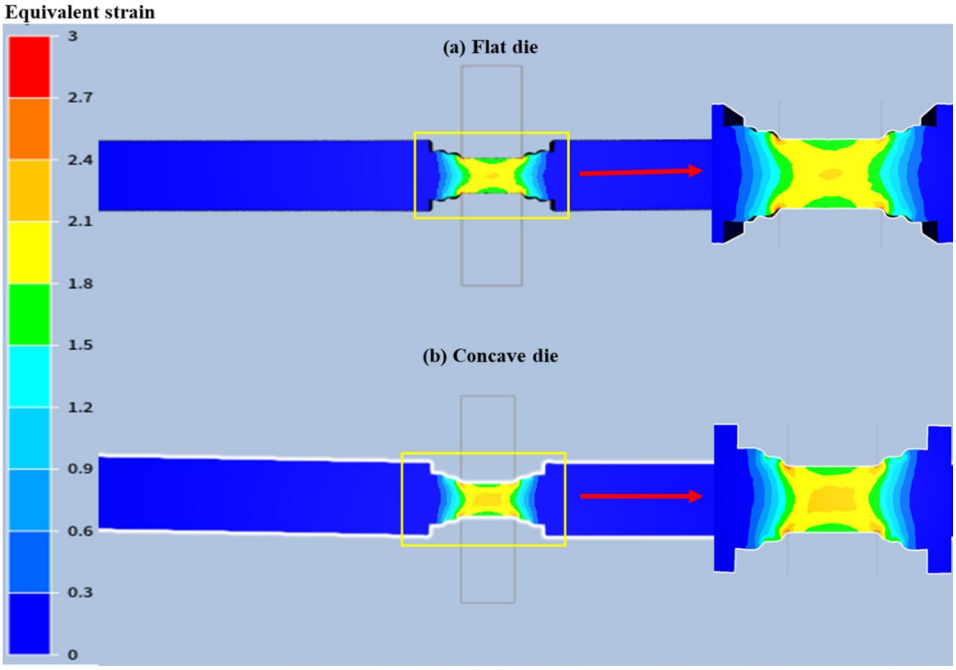

Fig. 6. Distribution of equivalent plastic strain after the multi-step deformation with: (**a**) Flat anvil and, (**b**) Concave anvil.

from 1.5 to 2.2, and concave anvils exhibited the higher strain level, ranging from 1.75 to 2.4. The concave dies could impart highest strain to a larger area at the core of the sample than the flat dies.

Employing a concave die during hot deformation constrains the material flow in the lateral direction. Due to this restriction, the concave die generates higher compressive stress and strain at the center of the workpiece compared to the flat anvils. Consequently, the use of a curved or angled anvil surface result in higher equivalent strain than that produced by a flat anvil. These results clearly demonstrate the strong relationship between die curvature and the resulting material flow behavior within the workpiece. Similar findings have also been reported in several published studies[5,6,12,19,37].

These observation aligns with previous research on the cogging process of AISI H13 steel, where similar trends were identified[12]. Furthermore, Du et al.[38] found that in forging a railway axle, concave anvils led to higher central strain (1.57) than flat anvils (1.35). Similarly, Xu et al.[39] demonstrated that a concave die profile enhanced compressive deformation. These results collectively demonstrate that die curvature influences not only the deformation path but also the magnitude and distribution of strain within the workpiece. Modifying the die curvature allows for effective control over both the pattern and extent of deformation. While existing literature primarily focuses on the effect of deformation path only on the strain distribution and research on the impact of deformation path on microstructure evolution and mechanical properties after multi-step deformation remains limited.

DRX volume fraction distribution

The FE analysis results reported in Fig. 7, show the distribution of DRX volume fraction. It can be seen that application of concave anvils generated higher DRX volume fraction compared to the flat anvils. Specifically, concave anvils give 85 to 100% of DRX volume fraction across cross section, while most of the cross section with flat anvil give between 60 and 70% DRX volume fraction. Therefore, concave anvils provide complete and homogenous distribution of DRX volume fraction.

This study findings corroborate previous research by Chen et al.[40], who demonstrated a link between homogenous deformation, higher deformation levels, and increased DRX volume fractions. Similarly, Muszka et al.[41] investigated the influence of different deformation paths on deformation and microstructural inhomogeneity in low carbon micro-alloyed steels during angular drawing. Their research revealed that complex deformation paths promote homogenous deformation and microstructural evolution, aligns with the

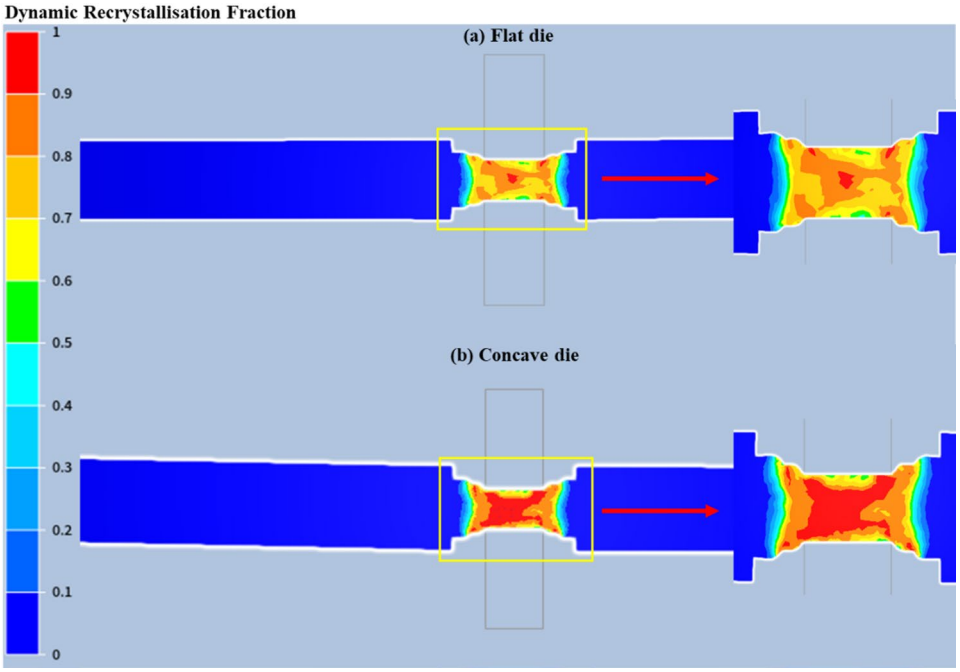

Fig. 7. Distribution of DRX volume fraction after the multi-step deformation with: (**a**) Flat anvil and, (**b**) Concave anvil.

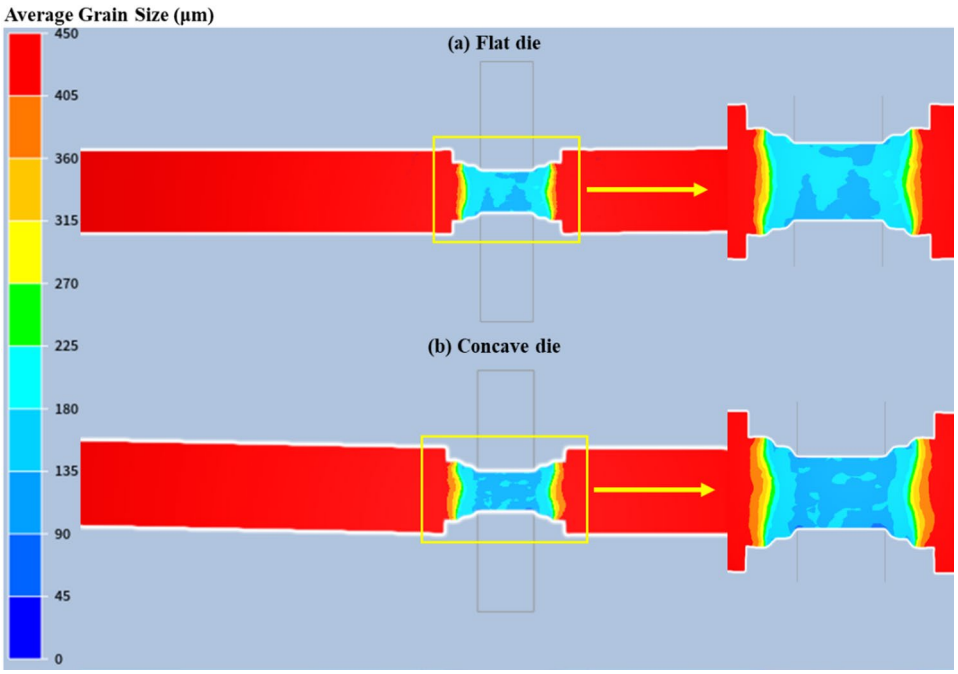

Fig. 8. Distribution of average grain size after the multi-step deformation with: (**a**) Flat anvil and, (**b**) Concave anvil.

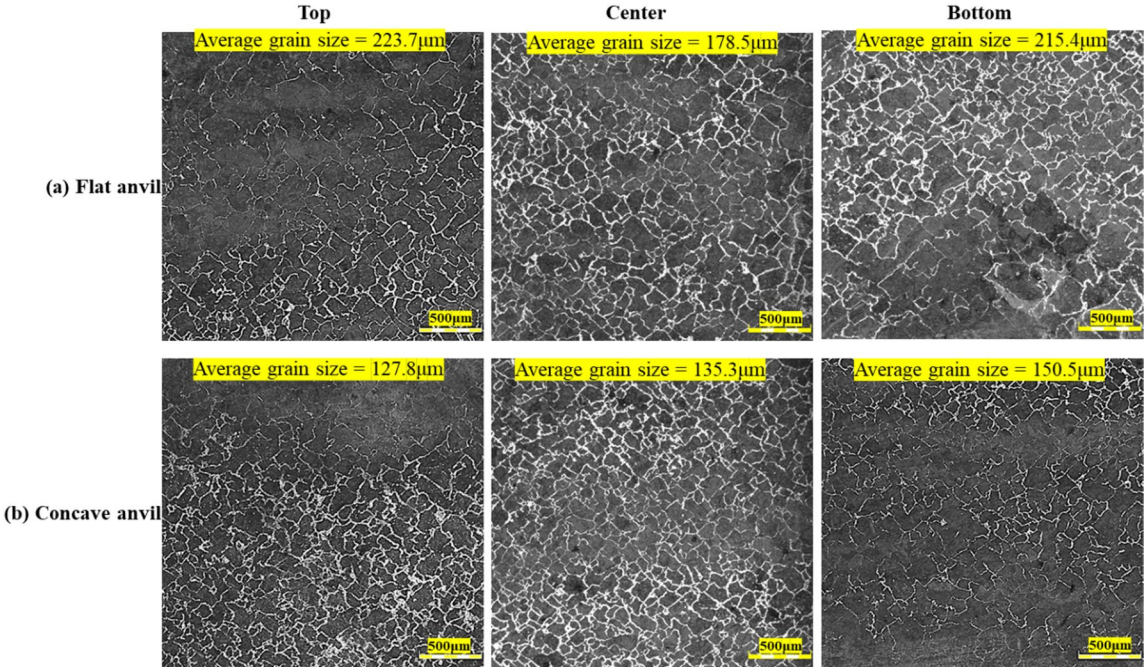

Fig. 9. Optical micrographs of specimens after multi-step deformation with: (**a**) Flat anvil and, (**b**) Concave anvil.

observations of this study. Both studies highlight the importance of deformation path complexity in achieving desirable microstructural characteristics. Nevertheless, existing literature primarily focuses on the influence of deformation paths on the distribution of dynamically recrystallized (DRX) fraction during single stage and uniaxial compression.

Average DRX grain size distribution

Figure 8 illustrate FE analysis results of the average grain size distribution. Before deformation, the initial average grain size was 450 μm, as measured after holding the sample at 1260 °C for 5 min. This value is representative of the grain size observed at the center of a large size forging, which is not desirable. After the multi-step deformation, the average DRX grain size predicted for flat and concave anvils was 190.5 μm and 143.7 μm, respectively. From Fig. 8(a) and 8(b), it is observed that concave anvils provide not only smaller grain sizes, but also, a more homogenous grain size distribution compared to the flat anvils, due to the complete DRX. Uniform and finer size grains endorse better mechanical properties.

Microstructure investigation and validation of FE model

Figure 9 presents optical micrographs taken at the top, center, and bottom along the central axis of each specimen. The micrographs show the average grain size at these locations, with the corresponding values indicated on the images for both deformation paths. The dead metal zone, or the region with coarser grains, is larger in the sample deformed using the flat anvil compared to the sample deformed with the concave anvil. At the specimen surface, friction with the anvil generates shear stresses that reduce effective plastic strain in that region. As a result, the surface undergoes lower levels of deformation, which inhibits dynamic recrystallization (DRX) and leads to coarser grains compared to the interior. The limited deformation is because of friction between the anvil and specimen. In contrast, the central region experiences higher effective plastic strain and therefore undergoes more complete DRX, resulting in finer and more equiaxed grains. Within the rest of the material, the grain size distributions appear similar for both anvils types. The average grain size for the specimens deformed with the flat and concave anvils was 178.5 μm and 135.3 μm respectively. As reported in Fig. 6, the equivalent strain varies from 1.5 to 2.4 from the surface to the center of specimen. The higher deformation level achieved with the concave anvils resulted in complete DRX and resulted in the finer DRX grains compared to the specimen deformed with the flat anvils.

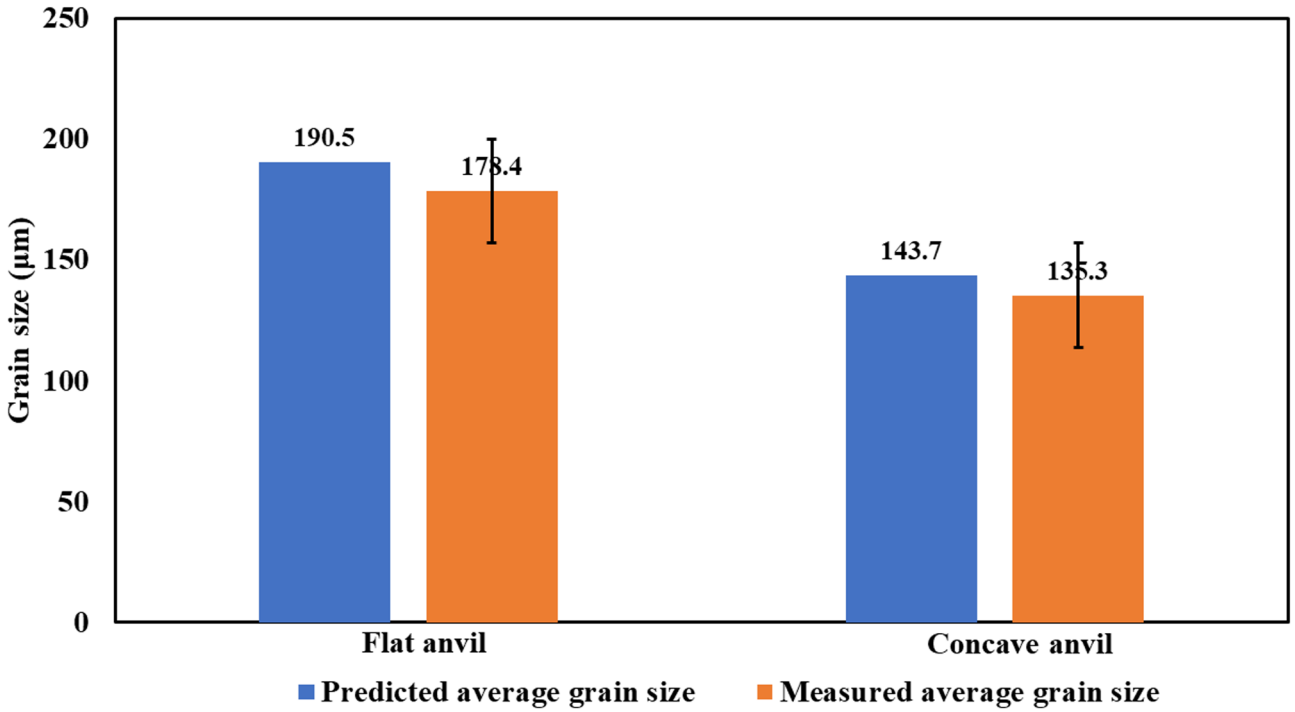

Fig. 10. Shows the accuracy between predicted and measured average grain size after the multi-step deformation with flat and concave anvil.

Figure 10 presents a comparison between the average predicted grain size and the measured grain size after multi-step deformation for central part of the specimen. The prediction accuracy for flat and concave anvils varies between 5.8% and 6.3% respectively, indicating good agreement between the predicted and measured values. Therefore, the developed FE model can effectively predict grain size evolution during the multi-step deformation process. Similar finding were reported in literature during the single stage deformation of steel, validation of measured and predicted data[14,34].

Hardness measurement and heterogeneity study

Figure 11 presents the hardness measurements for specimens subjected to multi-step deformation using flat and concave anvils. The y-axis represents the hardness values (HV), while the x-axis indicates the distance (in mm) from the respective surfaces. Hardness was measured at approximately 0.4 to 0.5 mm intervals along the vertical and horizontal axes, as well as along two diagonals (labeled 1 st and 2nd), as shown in the schematic. Additionally, the spacing between consecutive measurements was adjusted to ensure an equal number of data points along all four axes, enabling a more accurate comparison of hardness values. A load of 200 Kgf and a dwell time of 15 s were used for the hardness measurements. For the flat anvil, the hardness was found to be 643.6 ± 68.3 HV, while the concave anvil produced a hardness of 659.3 ± 41.6 HV. As discussed above, concave anvils produce a finer grain size compared to flat anvils. According to the Hall-Petch relationship, this smaller grain size translates to better mechanical strength in metallic materials[42,43]. The figure clearly demonstrates that the concave anvil resulted in more consistent hardness values, exhibiting less spread in hardness compared to the flat anvil.

A heterogeneity study, using the Coefficient of Variation (CoV) as heterogeneity index, was conducted on hardness values to identify an optimal deformation path used. The CoV, has been defined as the ratio of the standard deviation to the mean[44]. A CoV near zero indicates a homogeneous distribution, while a value of one represents maximum heterogeneity[45]. Figure 12 shows a clear trend of decreasing CoV values when progressing from flat to concave anvils, indicating improved homogeneity in hardness values distribution. The highest CoV (0.15) was associated with the flat anvil, while the lowest (0.06) corresponded to the concave anvil. As shown in Figs. 6 and 9, the concave anvils facilitated higher strain levels and more homogeneous distributions of both

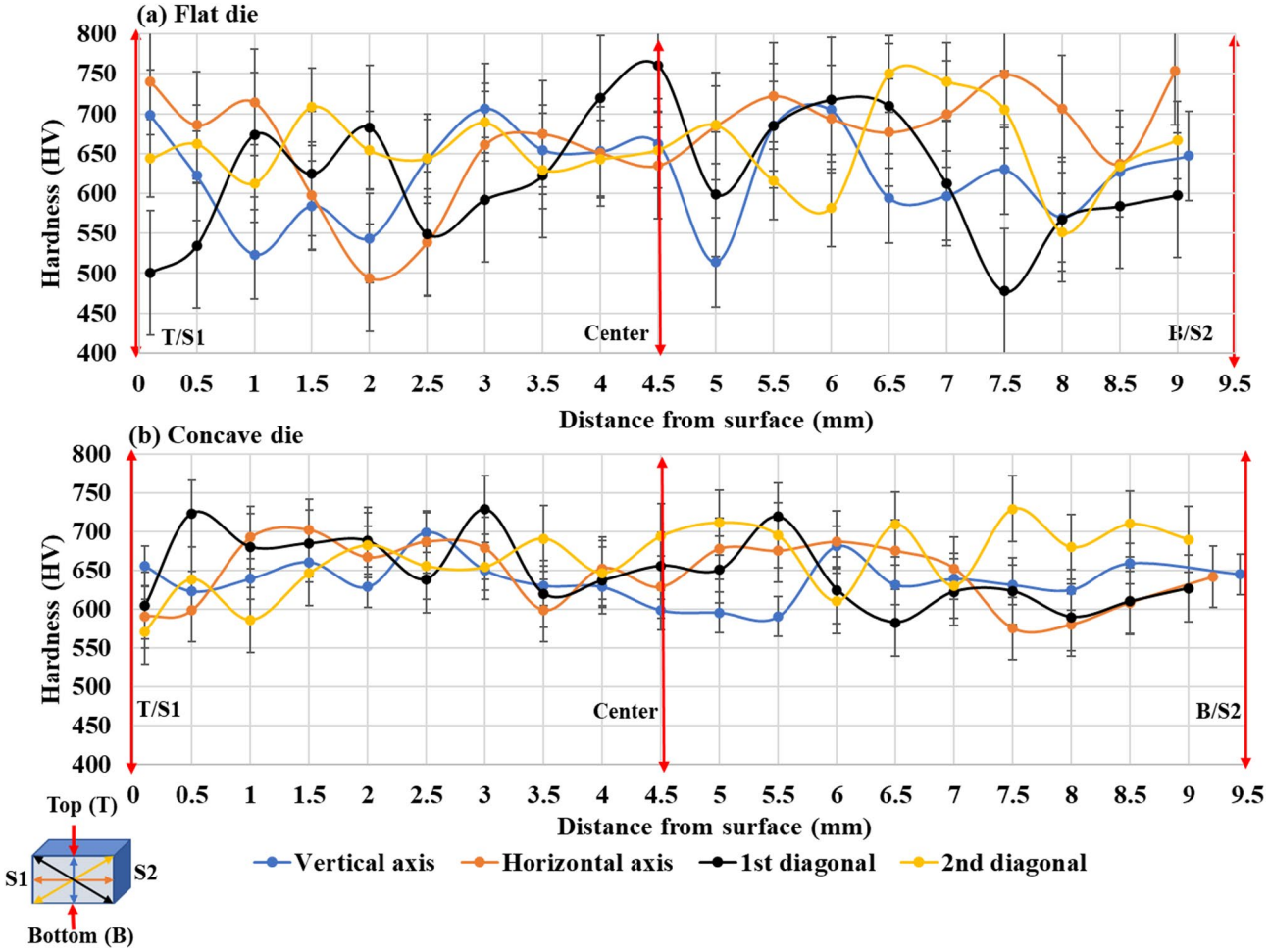

Fig. 11. Hardness measurement for multi-step deformed specimens with: (**a**) Flat anvils and, (**b**) Concave anvils.

strain and average grain size. These findings were consistent with studies reported in open literature[5,46,47]. The findings demonstrate that multi-step deformation using concave anvils results in more uniform hardness values compared to using flat anvils, due to the homogenous distribution of strain, DRX grain size and microstructure. Therefore, this study recommends the use of concave surface curvature dies for the multi-step forging of large industrial components in place of conventional flat surface dies.

Conclusions

This investigation combines experiments and FE analysis to study the influence of deformation paths on deformation. The evolution of microstructure and mechanical property was studied during the multi-step deformation of a high strength steel at 1150 °C and a strain rate of 0.01 s^{-1}. Two distinct deformation paths, defined by flat and concave anvils, were analyzed. The key findings and conclusions are summarized below:

(1) Both experimental and FE analysis results demonstrate that the deformation path significantly influences the level of deformation and microstructural evolution during multi-step deformation.
(2) Concave anvils promote higher and more uniform deformation, higher volume fraction of DRX and more uniform distribution of DRX grain size compared to flat anvil.
(3) Uniform hardness distribution was found on specimens deformed with the concave anvil.
(4) Concave anvils provide an optimal deformation path for the multi-step deformation process leading to improved forge quality.

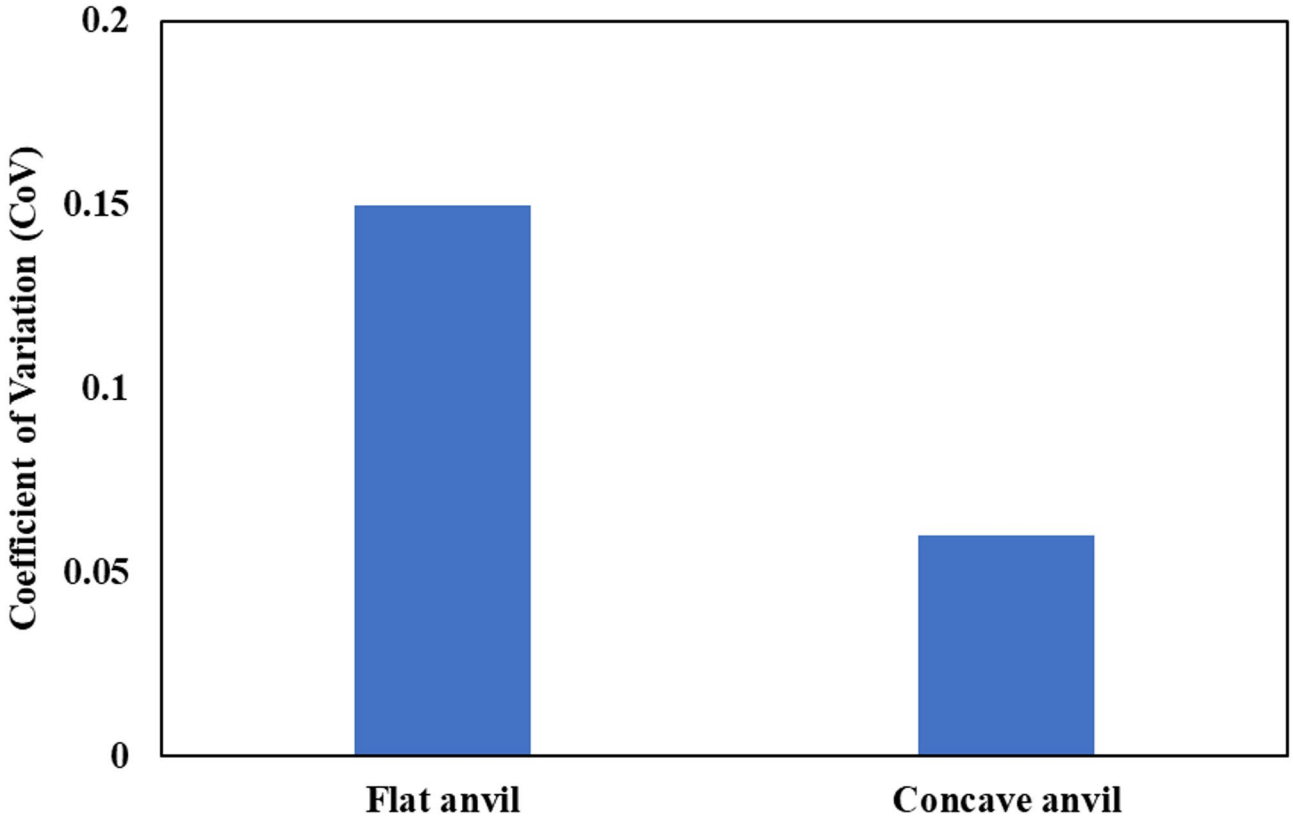

Fig. 12. The coefficient of variation for hardness values after the multi-step deformation process.

Data availability

The raw and processed data required to reproduce these results are currently unavailable, as they are being utilized in an ongoing study, but are available from the corresponding author on reasonable request.

Received: 30 May 2025; Accepted: 18 November 2025
Published online: 29 November 2025

References

1. Murugesan, M. & Jung, D. W. Two flow stress models for describing hot deformation behavior of AISI-1045 medium carbon steel at elevated temperatures. *Heliyon* **5**, e01347. https://doi.org/10.1016/j.heliyon.2019.e01347 (2019).
2. Chadha, K. & Microstructure Evolution Of Medium Carbon Low Alloy Steel During Ingot Breakdown Process by MANUSCRIPT-BASED THESIS PRESENTED TO ÉCOLE DE. *Dr. thesis Electron. Montr. École Technol. supérieure* (2018). https://espace.etsmtl.ca/id/eprint/2310
3. Mha, P. T., Dhondapure, P., Jahazi, M. & Tongne, A. Interpolation and extrapolation performance measurement of analytical and ANN-Based flow laws for hot deformation behavior of medium carbon steel. *Met. (Basel)*. 13. https://doi.org/10.3390/met13030633 (2023).
4. Harris, N., Shahriari, D. & Jahazi, M. Development of a fast converging material specific void closure model during ingot forging. *J. Manuf. Process.* **26**, 131–141. https://doi.org/10.1016/j.jmapro.2017.02.021 (2017).
5. Kukuryk, M. Analysis of deformation and microstructural evolution in the hot forging of the Ti-6Al-4V alloy. *Arch. Metall. Mater.* **60**, 597–604. https://doi.org/10.1515/amm-2015-0179 (2015).
6. Kukuryk, M. Experimental and numerical study of the closure of voids with different size and various locations in the three-dimensional cogging process. *Int. J. Mater. Form.* **17**, 1–15. https://doi.org/10.1007/s12289-023-01798-5 (2024).
7. Ahmadi, H., Dehghan, S. & Ranjbar, H. Enhancement of upsetting technology for minimizing internal defects in heavy ingot casting: simulation, optimization, and experimental validation. *Int. J. Mater. Form.* **18** (1), 21. https://doi.org/10.1007/s12289-025-01883-x (2025).
8. Zhang, Q. et al. Investigation of deformation behavior and strain – induced precipitations in Al – Zn – Mg – Cu alloys across a wide temperature range. *Sci. Rep.* 1–22. https://doi.org/10.1038/s41598-024-65669-y (2024).
9. Bontcheva, N. & Petzov, G. Microstructure evolution during metal forming processes. *Comput. Mater. Sci.* **28**, 563–573. https://doi.org/10.1016/j.commatsci.2003.08.014 (2003).
10. Ghodrati, N. et al. Influence of hot top height on macrosegregation and material yield in a Large-Size cast steel ingot using modeling and experimental validation. *Met. (Basel)*. **12** https://doi.org/10.3390/met12111906 (2022).
11. Dourandish, S., Champliaud, H., Morin, J. B. & Jahazi, M. Microstructure-based finite element modeling of a martensitic stainless steel during hot forging. *Int. J. Adv. Manuf. Technol.* **123**, 2833–2851. https://doi.org/10.1007/s00170-022-10306-z (2022).
12. Dhondapure, P. et al. Influence of deformation path on the stress state and damage evolution along the central axis of a large size forged ingot of AISI H13 steel. *J. Mater. Res. Technol.* **27**, 8244–8257. https://doi.org/10.1016/j.jmrt.2023.11.206 (2023).
13. Niu, L. & Zhang, Q. A void closure model based on hydrostatic integration and the lode parameter for additive manufacturing AlSi10Mg. *J. Manuf. Process.* **73**, 235–247. https://doi.org/10.1016/j.jmapro.2021.10.056 (2022).

14. Dhondapure, P., Rajakrishnan, N., Nayak, S. & Champliaud, H. Influence of deformation path on microstructure evolution during the open die forging of large size ingot of high strength steel: experiments and FE analysis. *Int. J. Adv. Manuf. Technol.* **134** (7), 3733–3750. https://doi.org/10.1007/s00170-024-14360-7 (2024).
15. Dasari, S. K. et al. Implementation of experimental static recrystallization of high strength steel into computational simulation of Multi-pass slab hot rolling. *Met. Mater. Int.* https://doi.org/10.1007/s12540-023-01442-6 (2023).
16. Dudra, S. P. & Im, Y. T. Analysis of void closure in open-die forging. *Int. J. Mach. Tools Manuf.* **30**, 65–75 (1990). 10.1016/0890–6955(90)90042-H.
17. Chegini, M., Aboutalebi, M. R., Seyedein, S. H., Ebrahimi, G. R. & Jahazi, M. Study on hot deformation behavior of AISI 414 martensitic stainless steel using 3D processing map. *J. Manuf. Process.* **56**, 916–927. https://doi.org/10.1016/j.jmapro.2020.05.008 (2020).
18. Cheng, J. Research on hot deformation characterization of a new weathering steel through processing map and microstructural observation. *Sci. Rep.* 1–17. https://doi.org/10.1038/s41598-025-86619-2 (2025).
19. Markov, O. E., Perig, A. V., Zlygoriev, V. N., Markova, M. A. & Grin, A. G. A new process for forging shafts with convex dies. Research into the stressed state. *Int. J. Adv. Manuf. Technol.* **90**, 801–818. https://doi.org/10.1007/s00170-016-9378-6 (2017).
20. Mandal, S., Jayalakshmi, M., Bhaduri, A. K. & Subramanya Sarma, V. Effect of strain rate on the dynamic recrystallization behavior in a Nitrogen-Enhanced 316L(N). *Metall. Mater. Trans. Phys. Metall. Mater. Sci.* **45**, 5645–5656. https://doi.org/10.1007/s11661-014-2480-1 (2014).
21. McQueen, H. J. Elevated-temperature deformation at forming rates of 10 – 2 to 102 s-1. *Metall. Mater. Trans. Phys. Metall. Mater. Sci.* **33**, 345–362. https://doi.org/10.1007/s11661-002-0096-3 (2002).
22. Jonas, J. J., Sellars, C. M. & Tegart, W. J. M. G. Strength and structure under hot-working conditions. *Metall. Rev.* **14**, 1–24. https://doi.org/10.1179/mtlr.1969.14.1.1 (1969).
23. Zhang, Y. et al. Processing maps for the Cu-Cr-Zr-Y alloy hot deformation behavior. *Mater. Sci. Eng. A*. **662**, 320–329. https://doi.org/10.1016/j.msea.2016.03.033 (2016).
24. Li, J. et al. Hot deformation and dynamic recrystallization in Al-Mg-Si alloy. *Mater. Charact.* **173**, 110976. https://doi.org/10.1016/j.matchar.2021.110976 (2021).
25. Nayak, S., Dhondapure, P., Singh, A. K., Prasad, M. J. N. V. & Narasimhan, K. Assessment of constitutive models to predict high temperature flow behaviour of Ti-6Al-4V preform. *Adv. Mater. Process. Technol.* **6**, 296–310. https://doi.org/10.1080/2374068X.2020.1731233 (2020).
26. Tize Mha, P., Dhondapure, P., Jahazi, M., Tongne, A. & Pantalé, O. Artificial neural Network-Based critical conditions for the dynamic recrystallization of medium carbon steel and application. *Met. (Basel).* **13** https://doi.org/10.3390/met13101746 (2023).
27. Christiansen, P., Hattel, J. H., Bay, N. & Martins, P. A. F. Physical modeling and numerical simulation of V-die forging ingot with central void. *Proc. Inst. Mech. Eng. Part. C J. Mech. Eng. Sci.* **228**, 2347–2356. https://doi.org/10.1177/0954406213517878 (2014).
28. Gruber, C. et al. Simulation of dynamic and meta-dynamic recrystallization behavior of forged alloy 718 parts using a multi-class grain size model. *Mater. (Basel).* **14**, 1–15. https://doi.org/10.3390/ma14010111 (2021).
29. Christiansen, P., Martins, P. A. F., Bay, N. & Hattel, J. H. Multi-objective optimization of die geometry in ingot forging. *Procedia Eng.* **81**, 2457–2462. https://doi.org/10.1016/j.proeng.2014.10.350 (2014).
30. Bechet, S. & Beaujard, L. New reagent for the micrographical demonstration of the austenite grain of hardened or hardened-tempered steels. *Rev. Met.* **52**, 830–836 (1995).
31. GEORGE F. VANDER VOORT. Revealing prior austenite grain boundaries. *Microsc Microanal.* **16**, 6–7. https://doi.org/10.1017/S14319276100 (2010).
32. Standard Test Methods for Determining Average Grain Size. *Astm E112-10* 13, 1–27; (2010). https://doi.org/10.1520/E0112-13R21.1.4
33. Ge, G. et al. Constitutive modeling of high temperature flow behavior in a Ti-45Al-8Nb-2Cr-2Mn-0. 2Y alloy. *Sci. Rep.* 1–9. https://doi.org/10.1038/s41598-018-23617-7 (2018).
34. Dourandish, S., Champliaud, H., Morin, J. B. & Jahazi, M. Numerical simulation and experimental validation of microstructure evolution during the upsetting process of a large size martensitic stainless steel forging. *Int. J. Mater. Form.* **17** https://doi.org/10.1007/s12289-024-01840-0 (2024).
35. Forge NxT 3. 2 user manual. (2023). https://www.transvalor.com/en/homepage doi:https://www.transvalor.com/en/homepage
36. Dudkiewicz, Ł. et al. Determination of the friction coefficient in the ring test for selected lubricants dedicated to the hot forging process of precision steel products. *Lubricants* **11**, 103390lubricants11090399 (2023).
37. Markov, O. E., Gerasimenko, O. V., Kukhar, V. V., Abdulov, O. R. & Ragulina, N. V. Computational and experimental modeling of new forging ingots with a directional solidification: the relative heights of 1.1. *J. Brazilian Soc. Mech. Sci. Eng.* **41**, 1–13. https://doi.org/10.1007/s40430-019-1810-z (2019).
38. Du, S. & Li, Y. Optimization of forging process parameters and anvil design for railway axle during High-Speed forging. *ASME Int. Mech. Eng. Congr Expo.* **57366**, 1–6. https://doi.org/10.1115/IMECE2015-50695 (2015).
39. Xu, Y. et al. Numerical modeling and anvil design of high-speed forging process for railway axles. *Int. J. Mater. Form.* **14**, 813–832. https://doi.org/10.1007/s12289-020-01590-9 (2021).
40. Chen, F., Ren, F., Chen, J., Cui, Z. & Ou, H. Microstructural modeling and numerical simulation of multi-physical fields for martensitic stainless steel during hot forging process of turbine blade. *Int. J. Adv. Manuf. Technol.* **82**, 85–98. https://doi.org/10.1007/s00170-015-7368-8 (2016).
41. Muszka, K., Madej, L. & Majta, J. The effects of deformation and microstructure inhomogeneities in the accumulative angular drawing (AAD). *Mater. Sci. Eng. A*. **574**, 68–74. https://doi.org/10.1016/j.msea.2013.03.024 (2013).
42. O Hall, E. The deformation and ageing of mild steel: III discussion of results. *Proc. Phys. Soc. Sect. B.* **64**, 747–753. https://doi.org/10.1088/0370-1301/64/9/303 (1951).
43. Petch Norman, J. The cleavage strength of polycrystals. *J. Iron Steel Inst.* **174**, 25–28 (1953).
44. Zhu, S., Yang, H., Guo, L. G. & Gu, R. J. Investigation of deformation degree and initial forming temperature dependences of microstructure in hot ring rolling of TA15 titanium alloy by multi-scale simulations. *Comput. Mater. Sci.* **65**, 221–229. https://doi.org/10.1016/j.commatsci.2012.07.014 (2012).
45. Nayak, S., Kumar Singh, A., Gokhale, H., Prasad, M. J. N. V. & Narasimhan, K. Optimization of Ti-6Al-4V ring rolling process by FE simulation using RSM. *Int. J. Solids Struct.* **262–263**, 112064. https://doi.org/10.1016/j.ijsolstr.2022.112064 (2023).
46. Kukuryk, M. & Winczek, J. Analysis of deformation and microstructure evolution during the cogging process of Waspaloy alloy. *MATEC Web Conf.* **157** https://doi.org/10.1051/matecconf/201815702022 (2018).
47. Hamad, K., Chung, B. K. & Ko, Y. G. Effect of deformation path on microstructure, microhardness and texture evolution of interstitial free steel fabricated by differential speed rolling. *Mater. Charact.* **94**, 203–214. https://doi.org/10.1016/j.matchar.2014.05.019 (2014).

Acknowledgements

We would like to thank Finkl Steel-Sorel, Canada, for the support and providing material for this research. We gratefully acknowledge Mr. Radu Romanica for his valuable assistance in precisely conducting the MaxStrain experiments.

Author contributions

Prashant Dhondapure: methodology, investigation, experiments and data analysis, writing original draft. Soumyaranjan Nayak: methodology, data curation, writing – review and editing. Simin Dourandish: methodology, resources, writing – review and editing. Mohammad Jahazi: Supervision, resources, conceptualization, funding acquisition, writing – review and editing.

Funding

This research was funded by Finkl Steel-Sorel, Canada, and MITACS under grant number [IT164670].

Declarations

Consent for publication

The authors confirm and provided consent for publication data of this research.

Conflict of interest

The authors affirm that there are no financial interests or personal relationships that could have influenced the findings presented in this paper.

Additional information

Correspondence and requests for materials should be addressed to P.D.